Ghost Diffraction: Causal Explanation via Correlated Trajectory Calculations

Bill Dalton*

Department of Physics, Astronomy and Engineering Science

St. Cloud State University

St. Cloud, MN 56301, USA

(February 1, 2008)

We use trajectory calculations to successfully explain two-photon "ghost" diffraction, a phenomenon previously explained via quantum mechanical entanglement. The diffraction patterns are accumulated one photon pair at a time. The calculations are based on initial correlation of the trajectories in the crystal source and a trajectory-wave ordering interaction with a variant generator inherent in its structure. Details are presented in comparison with ordinary diffraction calculated with the same trajectory model.

I. INTRODUCTION

In the "ghost" diffraction experiment of [1], photons correlated in a down conversion process are separated and then counted in coincidence after one photon passes through a slit mask. Strange as it may seem, the slit diffraction pattern is observed on the detection screen of the other photon if one only counts those pairs for which the first photon is detected by a small-aperature fixed detector. For this EPR [2] type experiment, the data was interpreted in [1] in terms of entangled states. A second and similar experiment [3] exhibited optical imaging via two photon coincidence counting. This experiment was likewise analyzed in terms of entangled states. In an earlier conference report [4] we have shown with detailed numerical calculations that "ghost" diffraction patterns can be explained by trajectory correlations assuming an initial position and velocity relationship for the particles.

*email: bdalton@stcloudstate.edu

In the present work, we give some detailed calculations of "ghost" diffraction patterns and examine trajectory details in comparison with those involved in deterministic explanations of ordinary diffraction. The trajectory calculations are carried out numerically using the trajectory-wave ordering interaction of [5,6]. The latter is a set of second order differential equations for trajectories which invoke, via solution, the integral method of generating random variants. We begin with a brief description of this particle-wave interaction.

II. TRAJECTORY-WAVE ORDERING INTERACTION (TWOI)

The TWOI studied earlier by the author, made use of a general line parameter [5,6]. The following equations represent a version with time as the independent variable.

$$\frac{d\dot{x}_i}{dt} - \frac{du_i}{dt} = -(\dot{x}_i - u_i)F \tag{1}$$

In these equation the x_i represent the particle coordinates, and $\dot{x}_i = dx_i/dt$. The u_i are components of a field ray-velocity and the function F is a real positive function of field components with units of inverse time. The field affects the trajectories only through the u_i and function F. The TWOI equations can be implemented with different choices for the u_i and function F, facilitating the study of different trajectory models. Specific expressions for u_i and F used in the diffraction calculations here are discussed in the following section. Modifications to impose metric constraints are discussed in [5,6].

The above set of trajectory equations has in general two important properties. First, the $\dot{x}_i$ approach the u_i as a limit. Second, in this limit $(\dot{x}_i \rightarrow u_i)$, (named the "attractor limit" in [5]) the large number distribution of the particles approaches the function F provided the initial particle phase-space values are chosen uniformly randomly over a large but not unique volume. The attractor limit is approached closer and closer as time increases. For practical calculations, one must set some criteria for "sufficiently close". These feature can be more easily seen with a simple one-dimensional case with $u_i = 0$. We directly integrate the following equation.

$$\frac{d\dot{x}}{dt} = -(\dot{x})F \tag{2}$$

This gives the following integral relations

$$\dot{x}(t) = \dot{x}(0) - \int_0^t F\dot{x}(t')dt' \tag{3}$$

$$\dot{x}(t) = \dot{x}(0) - \int_{x_0}^x F dx' \tag{4}$$

If we numerically solve (2) until the attractor limit $\dot{x}(t) \to 0$ is sufficiently satisfied, we obtain the following relation.

$$\int_{x_0}^x F dx' \cong \dot{x}(0) \tag{5}$$

Repeating this process many times with $(x(0), \dot{x}(0))$ chosen uniformly randomly over a sufficient volume of phase space, we generate a random variant specified by F. The quantity Fdx is proportional to the number of particles that reach the attractor limit $\dot{x}(t) \to 0$ between x and $x + dx$. It is a technique that indirectly invokes the integral method [7] to generate in the attractor limit a random variant specified by F . It re-arranges an initial distribution to match F. This interaction is viewed as one possible mechanism by which nature could bring about the observed relation between particle distributions and wave intensities.

To solve the trajectory equations we use both fourth and fifth order Runge-Kutta methods [5,8,9] with adaptive step size techniques [10,11]. These two methods are used as checks against each other. The adaptive step technique saves two to four orders of magnitude on net computation time. The system of second-order differential equations is reduced to a system of first-order differential equations following the method of Butcher [12,13]. Numerical details and a test case are given in the appendix of [5]. Figure 1 presents a histogram of particle positions in the attractor limit generated using (2) with $x(0) = -7$, $F = 0.3\exp(-.3|x|)\cos^2(2x)$, and $\dot{x}(0)$ chosen uniformly randomly from the range $(0, 1.2)$. The "sufficiently close" to the attractor limit criteria used was $|\dot{x}(t)| = 10^{-5}\max|\dot{x}(0)|$. The solid line in Fig. 1 gives the profile of F scaled to match the particle histogram. This distribution can also be generated with a wide variety of choices of the initial phase space volume. Use of random or a variety of amplitudes in F (instead of 0.3) together with a sufficiently large initial phase-space volume will still generate the same shape. The noise in the distribution is due to initializing with a random number generator, the "sufficiently close" criteria and numerical approximations.

The second property of the TWOI equations is the alignment feature of the particle velocities with the wave ray velocity. From (1) we can see that the rate that the attractor limit is approached depends on the initial velocity difference $(\dot{x}_i - u_i)$ and upon F. In Fig. 2 we give some representative trajectories with particles initialized at $Z = 10\lambda$ beyond a slit of width 10λ. The particles are initialized in directions at 20^0 intervals. One can see that the particles initially moving backwards can be turned around and approximately aligned up with the wave ray velocity in less than a wavelength.

The TWOI approach has some similiar features to, but some conceptional differences from, the deterministic approach initiated by Madelung [14] and de Broglie [15] and re-considered later by Bohm [16,17] and others [18] for the Schrodinger equation. In that work, the particle velocity $\dot{\vec{x}}$ is identified with the wave ray velocity so that the particles follow the wave flow tangent lines. We will refer to this case ($\dot{\vec{x}} = \vec{u}$) as the attached case. This attached case is approached in the attractor limit for the TWOI.

Critics of attached models quickly point out that the particle distribution must initially match the quadratic wave density, and that there is no mechanism to bring about the attached condition ($\dot{\vec{x}} = \vec{u}$). If initial conditions are met, the continuity equation guarantees that the distributions will continue to match. However, if tangent lines are initiated with a density that does not match the quadratic wave density, they will continue to differ. Interestingly, it was Bohm [16] who suggested using a force that depended on the difference ($\dot{\vec{x}} - \vec{u}$) to bring about the attached case as a limit. The TWOI can bring about this case as a limit, as well as generate in the particle distribution the wave intensity pattern if the latter is represented by F in the TWOI equations. The TWOI is a somewhat more general approach in that it does not depend upon a continuity equation, and F can represent any field intensity. Likewise, the $\vec{u}$ can be chosen in different ways, e.g., as a vector parallel to the Poynting vector as in [19], or as in the interesting work of Floyd [20].

III. SLIT DIFFRACTION

Slit diffraction has been observed for many types of particles, including photons, neutrons and atoms. Can slit diffraction be explained via calculating particle tra-

jectories, one particle at a time? One adamant view on this question is reflected in the well-known comment of Richard Feynman " a phenomenon which is impossible, absolutely impossible, to explain in any classical way, and which has in it the heart of quantum mechanics " [21]. By treating the wave as a field and using the TWOI, the author has been able to obtain slit diffraction patterns, one particle at a time. Here, we present a single, a double and a triple slit diffraction pattern in Figures 3, 4, and 5 respectively. These diffraction patterns are calculated using the following scalar wave equation $\nabla^2\Psi - k^2\Psi = 0$ and standard Rayleigh-Sommerfield diffraction [22] with Neumann boundary conditions together with the following equation for $\vec{u}$.

$$\vec{u} = -\imath\frac{A}{2}(\Psi^\dagger\vec{\nabla}\Psi - (\vec{\nabla}\Psi^\dagger)\Psi)/(\Psi^\dagger\Psi) \tag{6}$$

For light diffraction, we use $A = c/k$ where c is the speed of light. With (6) we are taking $\vec{u}$ proportional to the gradient of the phase of the complex field, as in the work of Madelung [14] and de Broglie [15]. The scalar field, together with its first and second partial derivatives needed in (1), are calculated numerically for each point along each trajectory. Because an adjustable step technique is used, the exact position where the trajectory crosses a screen is determined by using a fifth order Lagrange interpolation polynomial [23].

In each figure, the wave is calculated assuming a point source 500λ in front of the slits and a detector screen at 1000λ beyond the slits. For the single slit case shown in Fig. 3, the slit width is 8λ. In the double slit case shown in Fig. 4 , the slit width is 5λ and the center-to-center slit separation is 25λ . In the three slit case shown in Fig. 5 , the slit width is 5λ , and the center-to-center slit separation is 10λ. The solid lines in these figures represents the wave intensity scaled to match the histograms. From these figures, it is clear that slit diffraction patterns can be reproduced via deterministic trajectory calculations using the TWOI and treating the wave as a field.

It is instructive to view some typical trajectories. Figure 6 shows some typical trajectories for a three slit case with slit width of 5λ and slit center to center separation of 7λ. These trajectories are near the attractor limit at the slits, so that the trajectories closely represent the wave flow tangent lines. Notice that these trajectories are not straight lines and that the trajectories do not cross each other. These feature are characteristic of tangent line trajectories for waves involving the operator ∇^2 [24].

IV. TWO-PHOTON GHOST DIFFRACTION

Two-photon correlations involving slit diffraction have been measured using photon pairs made in a parametric down conversion process [1]. Figure 7a illustrates the experimental setup. The "unfolded" sketch is illustrated in Fig. 7b. These figures and notation follow Fig. 5 of Ref. [1] with some changes that feature the trajectory calculations here. The two polarization components are separated by a polarizing beam splitter into the "signal" beam and the "idler" beam as shown. The signal beam passes through a slit pattern onto a screen about a meter behind the slits. No slit pattern is placed in the idler beam. A small aperture detector D_1 is placed at a fixed position on the signal screen and a small aperture detector D_2 is used to scan the idler screen. Coincident two-photon measurements are made for signal-idler photon pairs if a signal photon enters the fixed detector D_1. After many pairs have been measured, the accumulated distribution on the idler screen clearly exhibits a slit diffraction pattern [1]. This is remarkable because no slit mask exist in the idler beam.

The author considers this to be one of the most intriguing experimental results of modern physics. It would appear that what happens to the signal photon is some how "known" by the idler photon. A two-photon entangled state explanation of the data distributions was given in [1]. Can this type of experiment be explained with a deterministic interactive particle-field model? To investigate this problem, we consider a very simple model whose features are best illustrated by the unfolded version sketch in Fig. 7 b. In this figure, as in [1] , the distance Z_2 is the distance from the slits back through the beam splitter BS to the crystal and then back along the idler path to the idler screen. The distance Z_0 is the distance from the crystal to the beam splitter and on to the slits. Z_1 is the distance from the slits to the fixed detector D_1.

We describe this system using our interacting particle-field model. The o-ray and e-ray polarization components satisfy the wave equations $\nabla^2 E_o - k^2 E_o = 0$ and $\nabla^2 E_e - k^2 E_e = 0$, and for both components we assume spherical wave solutions with sources centered at some point S in the crystal. The e-ray is diffracted by the slits and the o-ray continues to the idler screen. We likewise assume that together with the spherical wave, two particles are initialized at point S in the crystal with equal

and opposite velocity vectors [1]. For the e-ray we calculate the diffracted wave as in the slit diffraction described above, but here the source point S is generally not on the optical axis.

To calculate the particle trajectories we use Eqs. (1) and (6) with $A = c/k$, and $\Psi = E_o$ or $\Psi = E_e$. Our model crystal source is very thin in the Z direction and for each pair of particles, we choose the Y position of the source point S in the crystal uniformly randomly from a range of $(-W, W)$. The initial angular direction of the signal particle is likewise chosen uniformly randomly. However, the initial velocity direction of the idler particle is always fixed as the negative of the initial velocity direction of the signal particle (as viewed in the unfolded picture of Fig. 7b). This and the same initial position represent the initial trajectory coupling that gives rise to the "ghost" diffraction in this model. We first calculate the trajectory of the signal particle, and if it terminates in the aperture of detector D_1, we calculate the trajectory of the idler particle and record where it hits the idler screen. With this coincidence restriction, the accumulated histogram of idler particles on the idler screen is the "ghost" pattern in the language of [1]. An initial report by the author on this type of two-photon "ghost" diffraction calculations for a single and double slit case appears in a recent conference proceedings [4].

We show in Fig. 8 and Fig. 9 the "ghost" diffraction patterns calculated with this simple model for cases of one and three slits respectively. For both cases we used $Z_2 = 7000\lambda$, $Z_0 = 1000\lambda$, and $Z_1 = 500\lambda$. For the single slit case, shown in Fig. 8 we used a slit width of 15λ, a crystal half width of $W = 155\lambda$, and a 6λ aperture for the signal detector D_1. For the three slit case shown in Fig. 8, we used a slit width of 5λ, a slit center-to-center separation of 7λ, a crystal half width of $W = 215\lambda$, and a 10λ aperture for the detector D_1. It was necessary to calculate many signal trajectories because very few terminated on the narrow detector aperture of D_1.

The distinct recognizable diffraction patterns exhibited in Fig. 8 and Fig. 9 clearly indicate that two-photon "ghost" diffraction can be explained via deterministic trajectory calculations using the interacting particle-field model. This two-photon correlation phenomenon is a result of pattern selection via correlated trajectory selection. The trajectory correlations are entirely due to initial conditions. In Fig. 8 and Fig. 9 the solid line represents the diffraction pattern on the idler screen that results as if

one had a point source at the signal detector on the signal screen. The common features of the solid line and the histogram are due to the common geometry in the almost Fraunhofer limit. However, the patterns differ slightly from each other. This difference can be reasonably explained by the fact that the signal detector D_1 has a finite size. It is conceptually incorrect to think that the "ghost" diffraction is the result of a "collapsed probability" signal at D_1 propagating backwards to the idler screen.

In the conventional slit diffraction of Fig. 3, Fig. 4, and Fig. 5 the wave used for each particle had a common point source. By sharp contrast, each particle in the "ghost" diffraction generally is influenced by a different wave since the source positions in the crystal have a wide range $(-W, W)$. A random selection of signal trajectories just beyond the slits is shown in Fig. 10 for the three slit case. One can see that the trajectories cross each other and appear to have no definite pattern. In fact, if one accumulates a histogram on the signal screen, one finds a broad smear with no definite pattern. This is expected because each wave generally starts from a different source points in the crystal. However, it is in this very situation that we obtain the "ghost" diffraction pattern on the idler screen for that selection of signal trajectories that terminate in the fixed detector D_1. This feature is consistent with the observations in [1], in which the "ghost" patterns were obtained using rather divergent beams. By shifting the position of the detector D_1 we obtain a shifted "ghost" pattern on the idler screen. This corresponds to selecting an entirely different set of signal-idler trajectory pairs. The authors in [1] mentions that this interesting feature was observed in the experiment.

V. SUMMARY

We have made "ghost" diffraction calculations using a trajectory model with two key features. The first feature is the use of the TWOI equations to describe the trajectories. Through the TWOI, the diffracted field influences the distribution of the trajectory particles, one trajectory at a time. As a physical model both particle and field must be taken together. Here, the TWOI used to calculate the particle-field interaction is much closer to that of classical physics in which the particle is not "attached" to the field. This key freedom, not found in the "attached" models

initiated by Madlung [14] and de Broglie [15] many years ago, facilitates the random variant generator inherent in the structure of the TWOI to generate the wave intensity patterns in the ensemble distribution.

The second key feature is the initial velocity correlation of the photons in the down conversion crystal, as well as the same initial position. As the calculations clearly demonstrate, this initial coupling together with the TWOI is sufficient to give rise to the "Ghost" diffraction patterns. This is a simple classical trajectory model of this photon-photon experiment. Its success clearly lends support to a realistic and deterministic description of nature.

---

[1] Strekalov D.V., Sergienko A. V., Klyshko D. N., and Shih Y. H. (1993), Phys. Rev. Lett, 74 (18) 3600.

[2] Einstein A., Podolsky B., and Rosen N. (1935), Phys. Rev. 47, 777.

[3] Pittman T. B., Shih Y. H., Strakalov D. V., and Sergienko A. V. (1995), Phys. Rev. A 52,3429.

[4] Dalton B. J. (1998), in Causality and Locality in Modern Physics, Eds. G. Hunter, S. Jeffers, and J-P. Vigier, (Kluwer-Academic Publishers, Dordrecht, The Netherlands), 463.

[5] Dalton B. J. (1994), Deterministic Explanation of Quantum Mechanics Based on a New Trajectory-Wave Ordering Interaction, North Star Press of St. Cloud Inc., St Cloud, Minnesota.

[6] Dalton B. J. (1997), in The Present Status of the Quantum Nature of Light, Eds. S. Jeffers, S. Roy, J-P. Vigier, and G. Hunter,(Kluwer-Academic Publishers, Dordrecht, The Netherlands), 235.

[7] Rubinstein R. Y. (1981), Simulation and The Monte Carlo Method, Wiley and Sons, N. Y.

[8] Carnahan B.,Luther H. A. , Wilkes J. O. (1969), Applied Numerical Methods, John Wiley and Sons, N. Y., 366.

[9] Walters J.(1996), Commun. Ass. Comp Mach. 9 293.

[10] Kincaid D., Cheney W. (1990), Numerical Analysis, Brooks/Cole Publishing, Pacific Grove, California, 502 .

[11] Press W. H.,Flannery B. P., Teukolsky S. A., and Vetterling W. T.(1989), Numerical Recipes, The Art of Scientific Computing, Cambridge University Press, Cambridge CB2 IRP.

[12] Butcher J. C. (1964), J. Austral. Math. Soc. 4, 179.

[13] Butcher J. C. (1994), Computers in Physics, 8, (4) 411.

[14] Madelung E. (1926), Zeits. Phys.,40 332.

[15] de Broglie L. (1927), Compt. Rendus., 184, 273; 185, 380.

[16] Bohm D. (1952), Phys. Rev. 85 166; (1953), 89, 458.

[17] Bohm D. and Vigier J. V. (1954), Phys. Rev., 96, 208.

[18] Bohm D. and Hiley B. J. (1993), The Undivided Universe, Routhledge, London and New York. Many references to and summaries of earlier work can be found in this text.

[19] Prosser R. D., Jeffers S. and Sesroaches, J. (1997), in The Present Status of the Quantum Nature of Light, Eds. S. Jeffers, S. Roy, J-P. Vigier, and G. Hunter,(Kluwer-Academic Publishers, Dordrecht, The Netherlands), 151, This report list references to several related earlier studies.

[20] Floyd E. R. (1999), Int. J. Mod. Phys. A, 14, 111; See earlier references in this article.

[21] Feynman R. P., Leighton R. B. , Sands M.(1963), The Feynman Lectures on Physics, Vol. 1, Addison-Wesley, New York, 37.

[22] Goodman J. W.(1996), Introduction to Fourier Optics, McGraw-Hill, New York, 50.

[23] Henrica P. (1964), Elements of Numerical Analysis, John Wiley and Sons, Inc., New York, Ch. 9.

[24] Philippidis C., Dewdney C., and Hiley B. J. (1979), Nuovo Cimento B 52, 15.

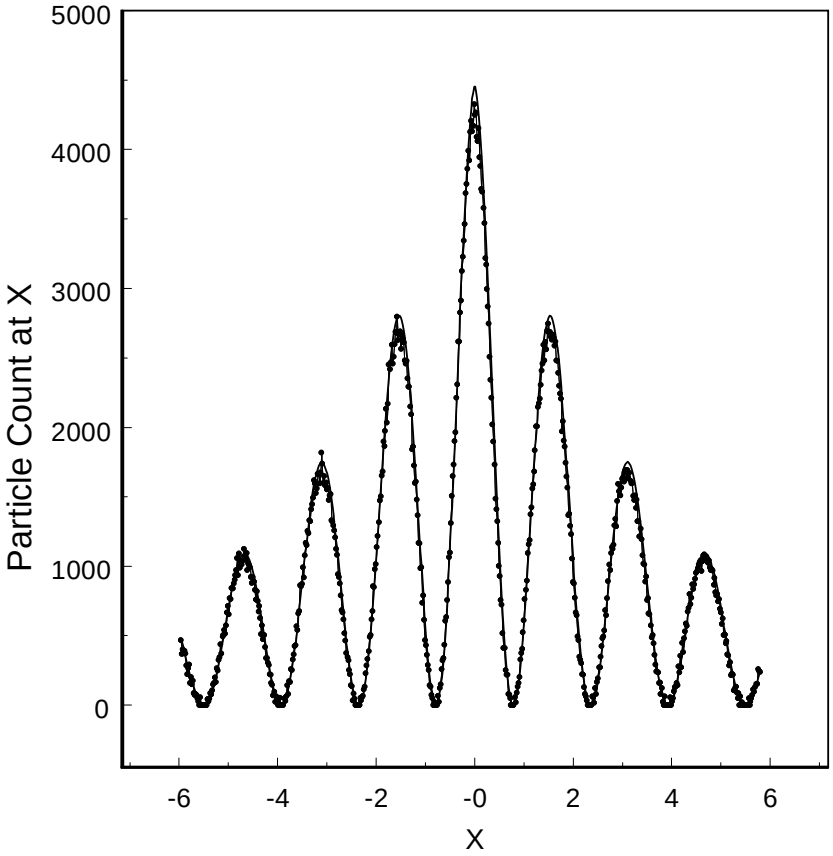

FIG. 1. A one dimensional histogram of particle count versus the X position in the attractor limit. The solid line is the shape of the function F scaled to approximately match the histogram.

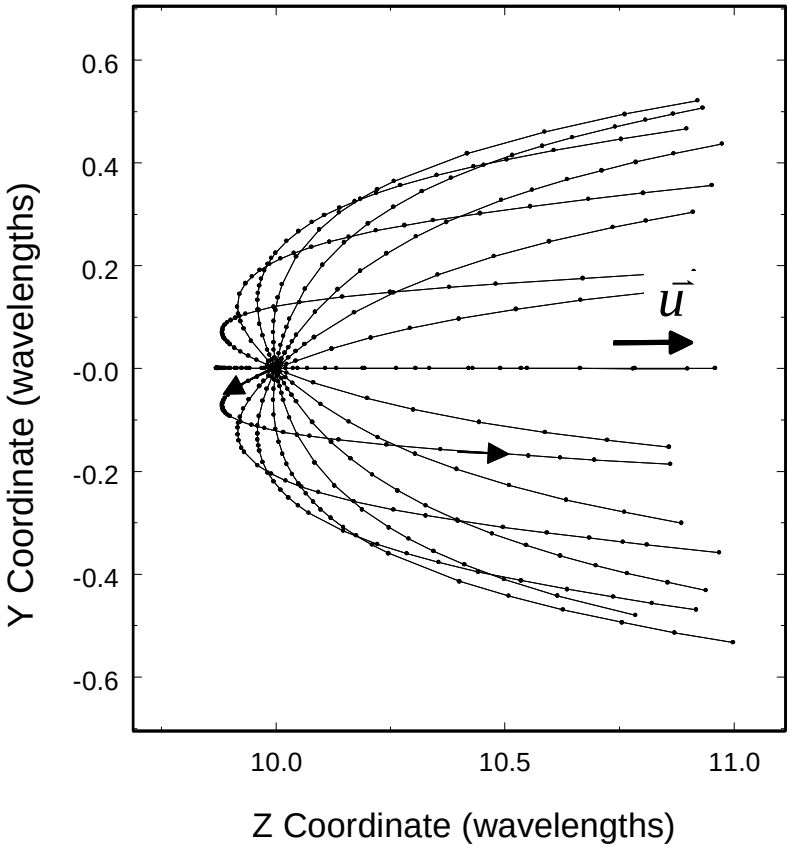

FIG. 2. Typical trajectories illustrating how the TWOI can bring about the attractor limit ($\dot{x}_i \rightarrow u_i$). The trajectories are initialized at the same point in directions at 20^0 intervals.

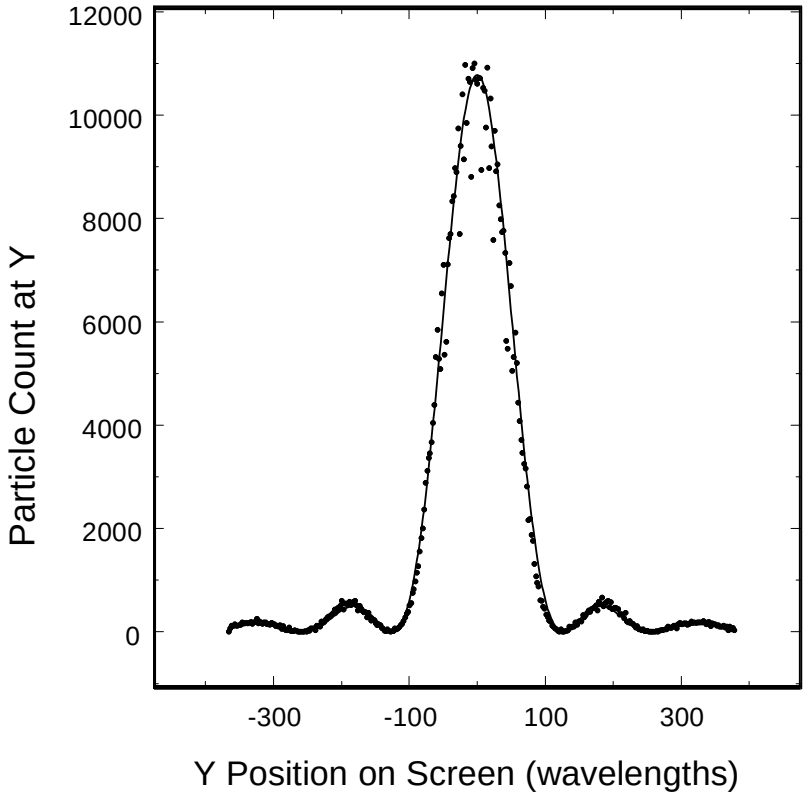

FIG. 3. Histogram of particle count versus the Y position on the detector screen for single slit diffraction. The trajectories of the particles were calculated one at a time. The solid line represents the wave intensity curve scaled to approximately match the histogram.

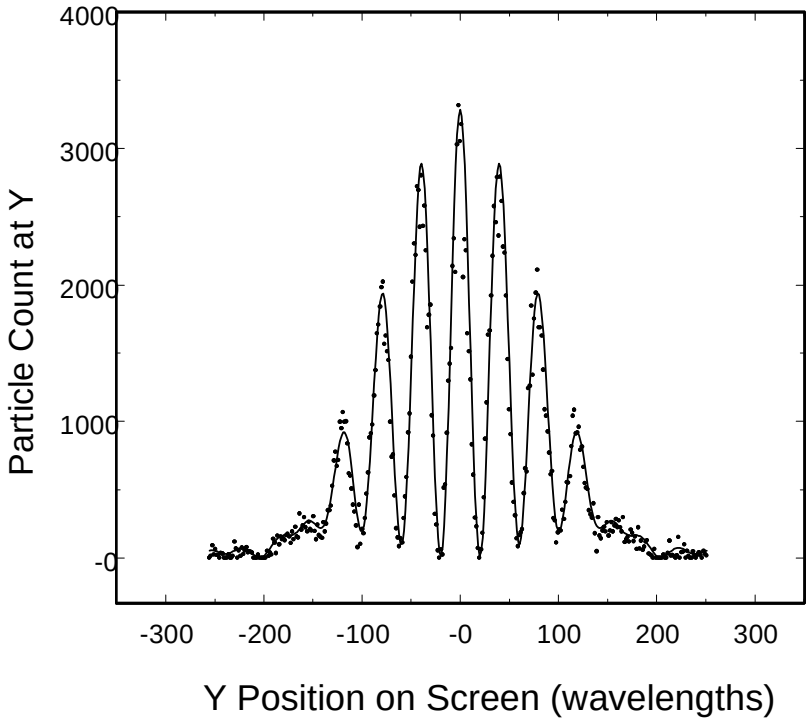

FIG. 4. Histogram of particle count versus the Y position on the detector screen for double slit diffraction. The trajectories of the particles were calculated one at a time. The solid line represents the wave intensity curve scaled to approximately match the histogram.

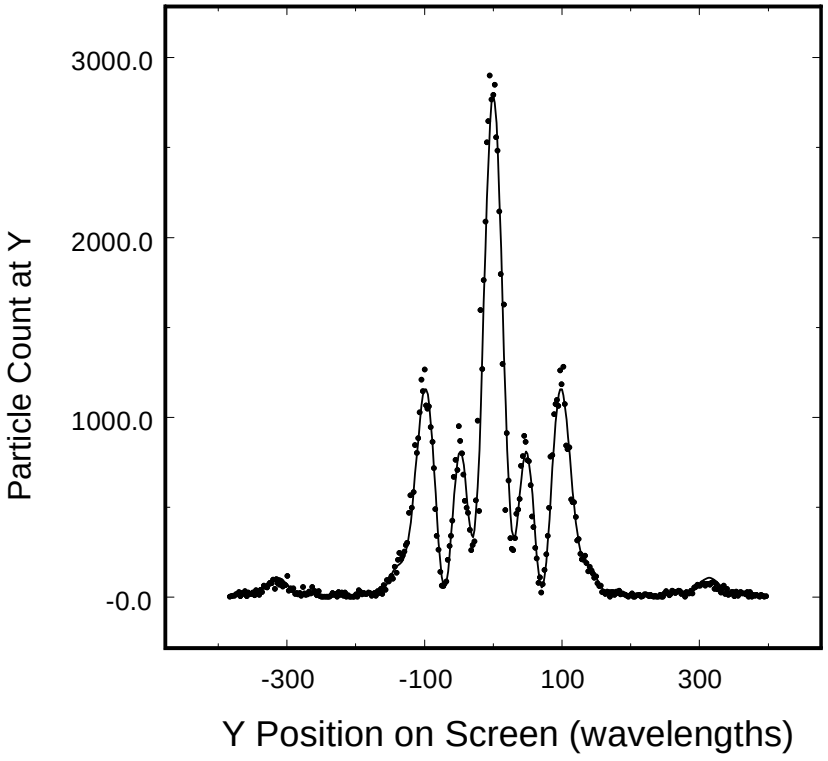

FIG. 5. Histogram of particle count versus the Y position on the detector screen for three-slit diffraction. The trajectories of the particles were calculated one at a time. The solid line represents the wave intensity curve scaled to approximately match the histogram.

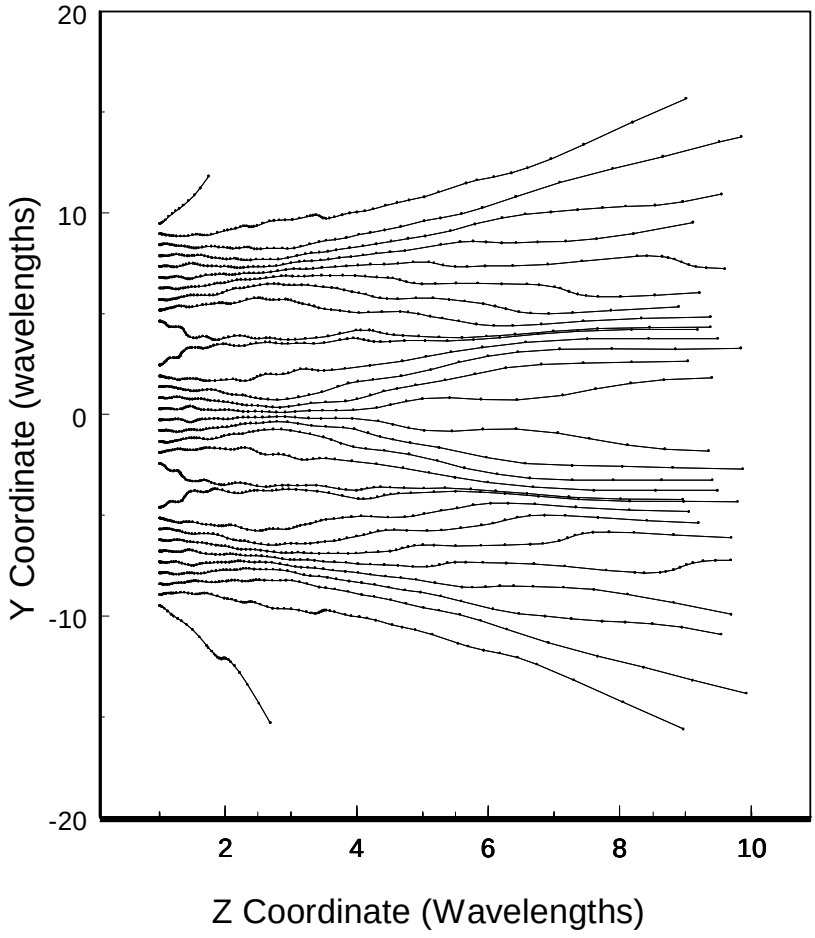

FIG. 6. A selection of typical trajectories in the attractor limit in the very near field region for three-slit diffraction. The dots on the lines represent the adjustable step positions. The trajectories are not straight lines and do not cross each other.

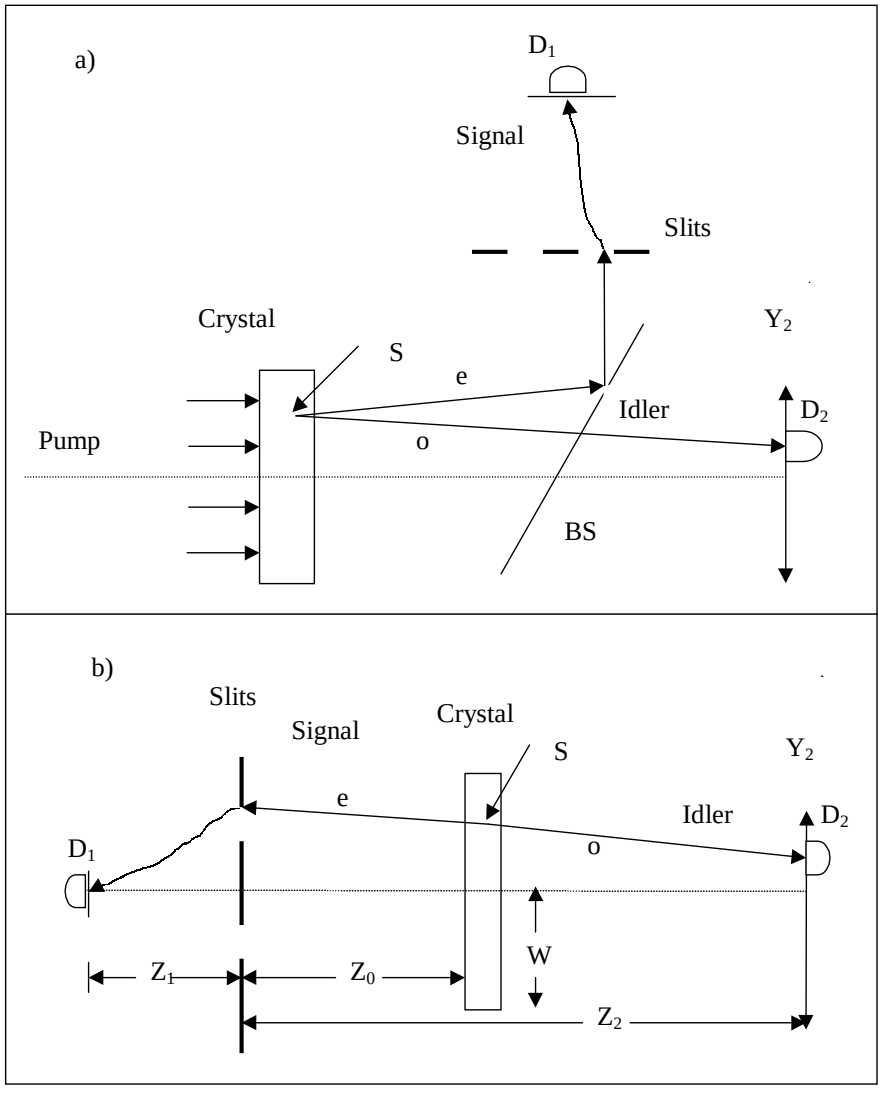

FIG. 7. Schematic (a) illustrates the experimental setup and calculation model for "ghost" diffraction, and schematic (b) illustrates the unfolded view following Fig. 5 of [1]. Detectors D1 and D2 measure the signal and idler photons in coincidence. D1 is fixed and D2 is scanned. The diffraction pattern is observed on the idler screen whereas the signal screen is behind the slits.

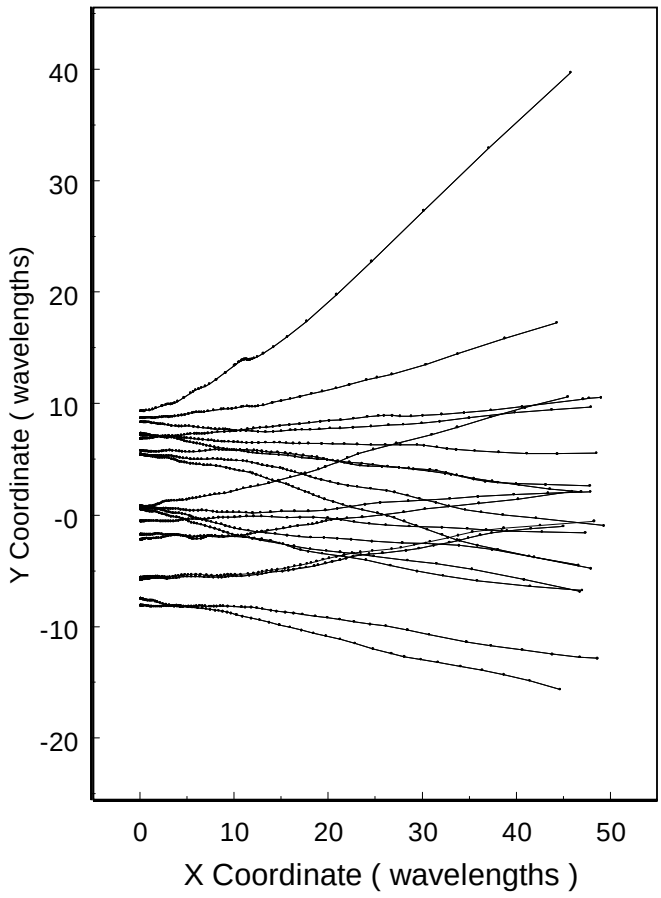

FIG. 8. A random selection of signal trajectories just beyond the three-slit mask. Even though the particle is each case is near the attractor limit, the trajectories can cross each other because each is influenced by a wave from a different point source location in the crystal. The "ghost" diffraction pattern arises from those idler trajectories paired with just the very small fraction of signal trajectories that terminate on the small detector D_1.

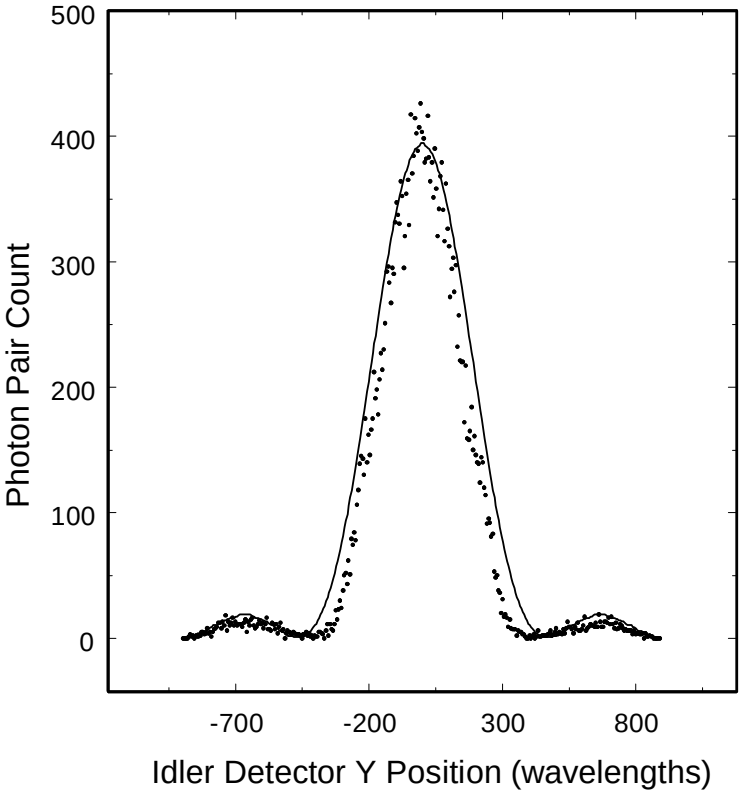

FIG. 9. A single slit "ghost" diffraction pattern. Histogram of photon pair count versus Y position on the idler screen. The correlated signal and idler trajectory pairs are calculated one at a time. The solid line represents a diffraction curve calculated on the idler screen as though one had a point source at the signal detector.

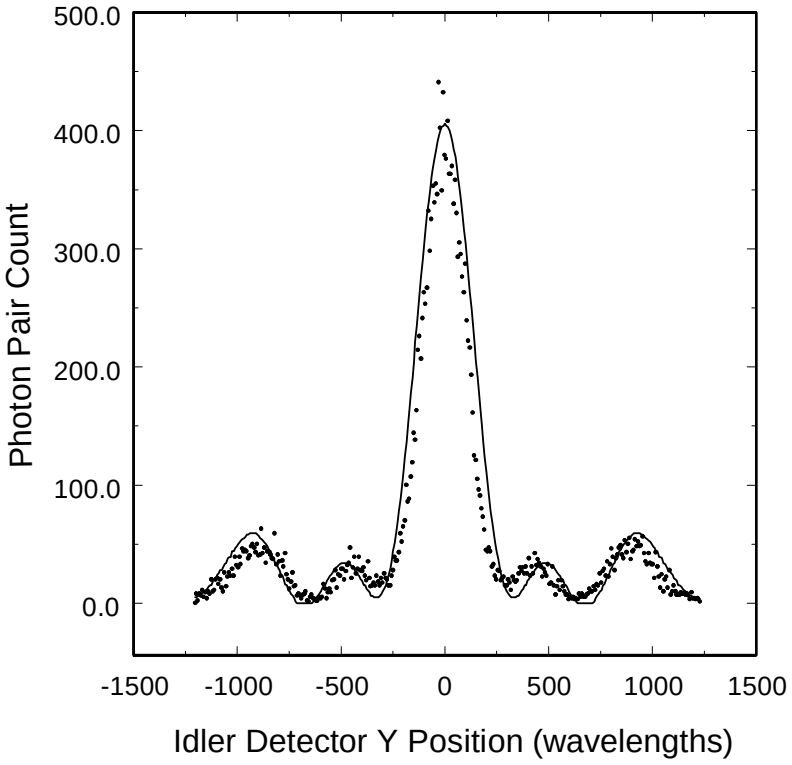

FIG. 10. A three slit "ghost" diffraction pattern. Histogram of photon pair count versus Y position on the idler screen. The correlated signal and idler trajectory pairs are calculated one at a time. The solid line represents a diffraction curve calculated on the idler screen as though one had a point source at the signal detector.